NASA/TM-20205008042

DGEN Aeropropulsion Research Turbofan Source-Diagnostic Test: Experimental Setup and Acoustic-Data Structure

Lennart S. Hultgren, Devin K. Boyle, and Brenda S. Henderson
Glenn Research Center, Cleveland, Ohio

October 2020

NASA STI Program . . . in Profile

Since its founding, NASA has been dedicated to the advancement of aeronautics and space science. The NASA Scientific and Technical Information (STI) Program plays a key part in helping NASA maintain this important role.

The NASA STI Program operates under the auspices of the Agency Chief Information Officer. It collects, organizes, provides for archiving, and disseminates NASA's STI. The NASA STI Program provides access to the NASA Technical Report Server—Registered (NTRS Reg) and NASA Technical Report Server—Public (NTRS) thus providing one of the largest collections of aeronautical and space science STI in the world. Results are published in both non-NASA channels and by NASA in the NASA STI Report Series, which includes the following report types:

- TECHNICAL PUBLICATION. Reports of completed research or a major significant phase of research that present the results of NASA programs and include extensive data or theoretical analysis. Includes compilations of significant scientific and technical data and information deemed to be of continuing reference value. NASA counter-part of peer-reviewed formal professional papers, but has less stringent limitations on manuscript length and extent of graphic presentations.

- TECHNICAL MEMORANDUM. Scientific and technical findings that are preliminary or of specialized interest, e.g., "quick-release" reports, working papers, and bibliographies that contain minimal annotation. Does not contain extensive analysis.

- CONTRACTOR REPORT. Scientific and technical findings by NASA-sponsored contractors and grantees.

- CONFERENCE PUBLICATION. Collected papers from scientific and technical conferences, symposia, seminars, or other meetings sponsored or co-sponsored by NASA.

- SPECIAL PUBLICATION. Scientific, technical, or historical information from NASA programs, projects, and missions, often concerned with subjects having substantial public interest.

- TECHNICAL TRANSLATION. English-language translations of foreign scientific and technical material pertinent to NASA's mission.

For more information about the NASA STI program, see the following:

- Access the NASA STI program home page at http://www.sti.nasa.gov

- E-mail your question to help@sti.nasa.gov

- Fax your question to the NASA STI Information Desk at 757-864-6500

- Telephone the NASA STI Information Desk at 757-864-9658

- Write to:
  NASA STI Program
  Mail Stop 148
  NASA Langley Research Center
  Hampton, VA 23681-2199

NASA/TM-20205008042

DGEN Aeropropulsion Research Turbofan Source-Diagnostic Test: Experimental Setup and Acoustic-Data Structure

Lennart S. Hultgren, Devin K. Boyle, and Brenda S. Henderson
Glenn Research Center, Cleveland, Ohio

National Aeronautics and
Space Administration

Glenn Research Center
Cleveland, Ohio 44135

October 2020

Acknowledgments

Many thanks to the NASA Glenn Research Center Aero-Acoustic Propulsion Laboratory staff for their expertise and dedication in preparing and executing the 2019 test campaign.

This work was sponsored by the Advanced Air Vehicle Program
at the NASA Glenn Research Center

Trade names and trademarks are used in this report for identification only. Their usage does not constitute an official endorsement, either expressed or implied, by the National Aeronautics and Space Administration.

Level of Review: This material has been technically reviewed by technical management.

Available from

NASA STI Program
Mail Stop 148
NASA Langley Research Center
Hampton, VA 23681-2199

National Technical Information Service
5285 Port Royal Road
Springfield, VA 22161
703-605-6000

This report is available in electronic form at http://www.sti.nasa.gov/ and http://ntrs.nasa.gov/

DGEN Aeropropulsion Research Turbofan Source-Diagnostic Test: Experimental Setup and Acoustic-Data Structure

Lennart S. Hultgren, Devin K. Boyle, and Brenda S. Henderson
National Aeronautics and Space Administration
Glenn Research Center
Cleveland, Ohio 44135

Abstract

The experimental setup of, and available data from a recent core/combustor-noise source-diagnostic test utilizing a small turbofan engine are described. The 2019 test campaign continued the investigation of the core/combustor-noise component of aircraft-propulsor noise begun in an earlier baseline test, but with a more extensive acoustic-instrumentation layout. The purpose of both tests was to better understand the impact on civilian-transport airport-community noise from turbofan-combustor sources and thereby to lay the foundation for improved noise-prediction methods and noise-mitigation techniques. Simultaneous high-data-rate acoustic measurements were obtained using a circumferential sensor array at the core-nozzle exit in conjunction with sideline and farfield microphone arrays. The test matrix contained engine operational points from engine idle to maximum power and was repeated for different circumferential and sideline array configurations, as well as for redundancy. The extensive data set (up to 93 channels of data and various configurations) allows the application of advanced source-separation and phased-array methods to elucidate not only the core-noise structure, but also the propagation characteristics of other propulsion noise sources. The present report provides a detailed description of the different test points, their associated instrumentation layouts, and the structure of the acquired data set. Results from various data analyses are reported separately.

1 Introduction

Propulsion systems for far-term ultra-efficient commercial subsonic transport aircraft, when compared to current advanced designs, are expected to have an increasingly higher bypass ratio (BPR), from larger fans combined with much smaller cores, and to have high-efficiency, ultra-clean burning, fuel-flexible combustors [1]. The increased BPR, expected aircraft configuration changes, and advances in fan-noise mitigation are expected to reduce the non-core propulsion-noise sources for all aircraft-engine operating conditions. To meet the required efficiency and emissions goals and to fit within the space available for the core, far-term combustor architectures may well turn out to be drastically different than those of current advanced through proposed mid-term generation combustors. The impact of these yet to be fully developed advanced techniques and architectural changes on combustor noise is not known at present, but could lead to a strengthening of its sources. Consequently, unless effective noise-reduction strategies are developed, combustor noise is likely to become a prominent contributor to overall airport community noise. This environmental impact is an issue of great importance not only to future gas-turbine propulsors, but also to proposed far-term hybrid-electric aircraft-propulsion systems.

The NASA core/combustor-noise research efforts are aimed at obtaining a better understanding of propulsion-noise sources (in particular those associated with the combustor) and their impact on the farfield noise signature. The ultimate goal is to enable improved turbofan noise-prediction methods as well as noise-mitigation techniques. This report describes the experimental setup and available acoustic data from the July–August 2019 DGEN Aeropropulsion Research Turbofan (DART) source-diagnostic test (SDT) in the anechoic Aero-Acoustic Propulsion Laboratory (AAPL) at NASA Glenn Research Center (GRC). DART is a cost-efficient testbed for the study of core- noise physics and mitigation. The SDT campaign continued the exploration and documentation of the DART core/combustor noise begun in an earlier baseline test [2], but with more extensive instrumentation.

2 Experimental Setup

The center piece of DART is an AKIRA MecaTurbines DGEN 380 turbofan engine—originally developed by Price Induction for the personal-light-jet market, but not certified.[a] It is a two-spool 500 lbf (2.2 kN) thrust-class geared turbofan engine with a bypass ratio of approximately 7.6. The fan rotor has 14 wide-chord blades and is geared down from the single-stage uncooled axial low-pressure turbine by a ratio of 3.32. A single-stage high-pressure centrifugal compressor is directly driven by an uncooled single-stage axial high-pressure turbine. Jet-A fuel is burned in a conventional reverse flow annular combustor. The DGEN 380 modular design allows the replacement of major components with parts modified for invasive instrumentation with comparative ease. Even though it is a rather small turbofan engine, its acoustic signature is relevant to large commercial aircraft engines [3, 4].

The AAPL facility at NASA GRC is a hemispheric dome with a radius of about 20 m (65 ft) with acoustic treatment on the walls and floor. The treatment consists of fiberglass wedges, with a 0.61 m (2 ft) depth, resulting in an anechoic lower limit of approximately 150 Hz. The DART was positioned near the center of the facility allowing the use of the existing AAPL overhead microphone-mounting points. Figure 1 shows the DART and the overhead and sideline-microphone arrays in AAPL. During normal operation the door on the far right is open to allow engine exhaust to exit the facility. The coordinate system used to describe measurement locations is a spherical one with its origin located on the engine centerline at the core-nozzle exit plane. The polar angle is zero in the inlet direction and the azimuthal angle is zero in the engine port-side (left-hand side facing forward) horizontal plane. The acoustic-sensor coordinates are described in more detail in Appendix A.

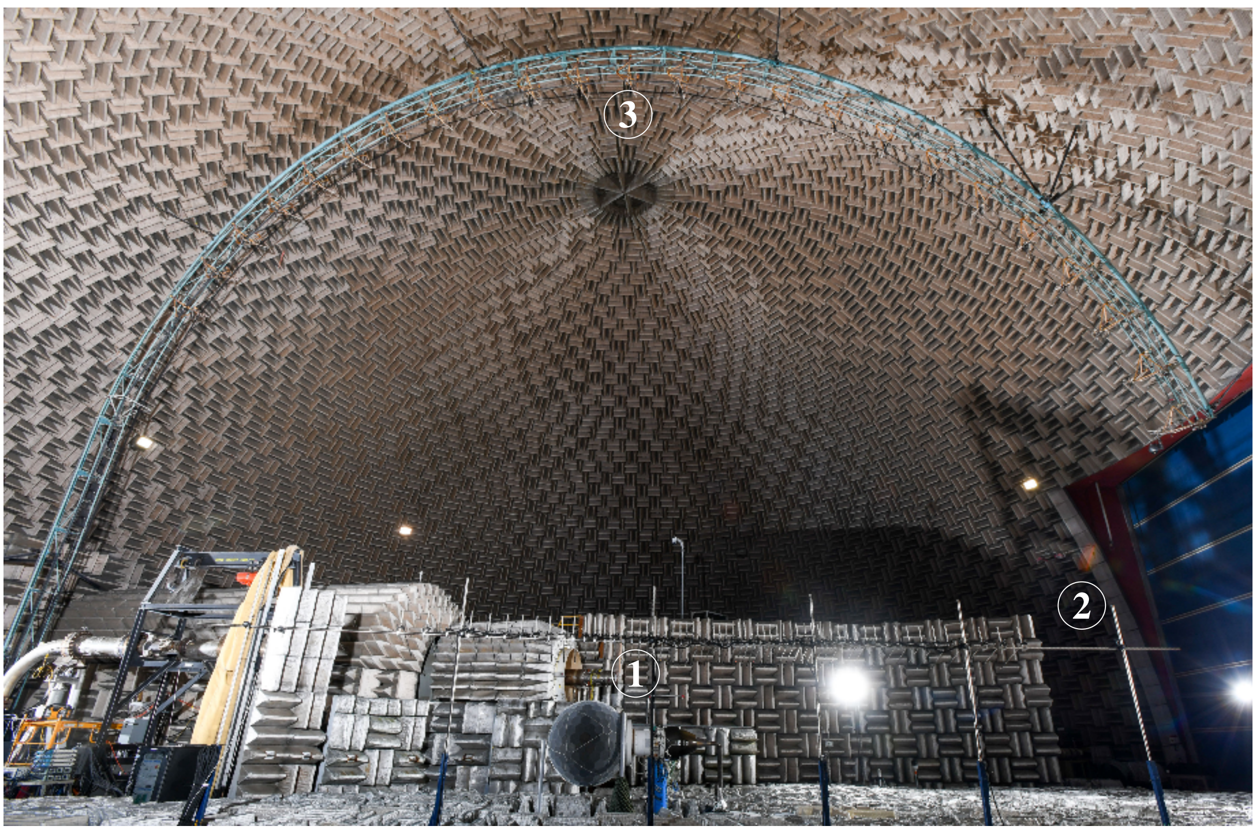

Figure 1. DART ①, sideline ② and overhead ③ arrays

[a]Title 14 Code of Federal Regulations Part 33, United States of America (e-CFR)

2.1 *Farfield (Overhead) Microphone Array*

The existing 24 microphone locations of the AAPL overhead array (see 3 in Fig. 1) were utilized in this test. The microphones were oriented such that their faces pointed at the center of the core-exhaust plane. The overhead-array microphones are labeled as sensors FF001 through FF024, with the 'FF' indicating farfield and the numerical part increasing with aft position. Note that both the radial distance from the engine-core exit and the azimuthal angle vary with the polar angle of the microphone position since the 'design origin' of the overhead-array is fixed with respect to the AAPL Nozzle Acoustic Test Rig (NATR) [5] seen in the background of Fig. 1. Panels (a) and (b) in Fig. 2 show the radial distance, normalized by the core-nozzle-exit outer diameter, 0.229 m (9.02 inch), and the azimuthal angle, both versus the polar angle for the microphones. The polar angles fall in the approximate range of 42–150°. The nondimensional radial distance falls in the range of about 48–74. According to the criteria given by Ahuja [6], the overhead microphones are located in the geometric farfield. The azimuthal angles of the overhead-array microphones vary due to the out-of-azimuthal-plane rotation of the array in the current coordinate system.

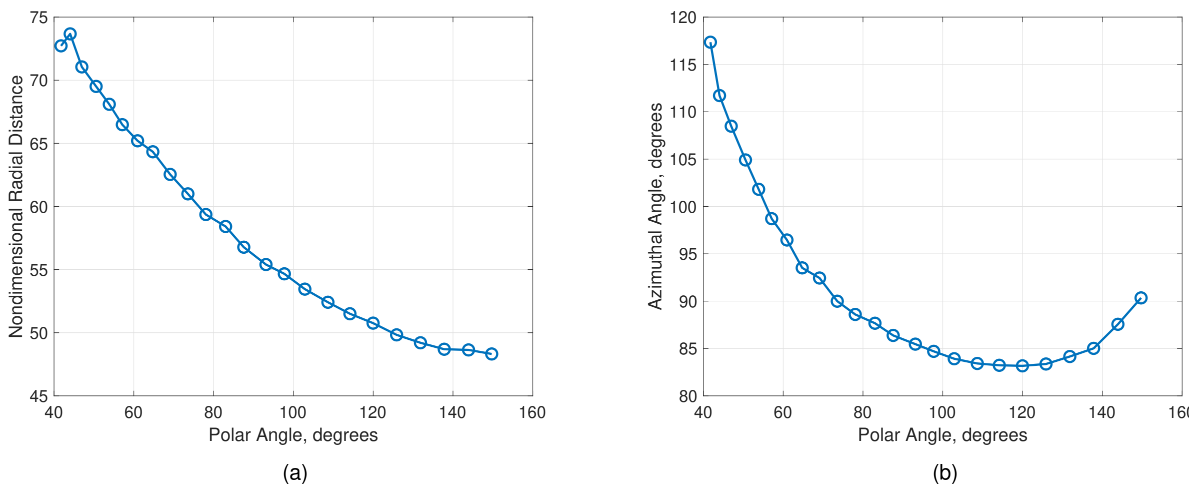

Figure 2. AAPL overhead microphone array: (a) microphone nondimensional radial distance versus polar angle; (b) microphone azimuthal angle versus polar angle

The overhead array was populated with Brüel & Kjær type 4939 1/4-inch externally polarized free-field microphones. The polarization voltages were supplied by 6 four-channel Brüel & Kjær NEXUS 2690-A-OS4 microphone conditioning amplifiers. Each NEXUS channel was set to unity gain. The channels are A/C coupled by design, but have a number of selectable highpass filters. The minimum highpass cut-off frequency value of 0.1 Hz was used.

2.2 *Sideline Microphone Arrays*

In addition to the microphones mounted in the overhead array, two alternate sideline microphone arrays were also utilized. These will be referred to as the 'sideline-088' and 'sideline-148' arrays (or LA088 and LA148 when brevity of notation is desired). Figure 3 shows an aft-quadrant view of the sideline-088 microphone array. Because it was desired to acquire data simultaneously for the overhead and sideline arrays, the preferable ground-based-microphone hard-surface arrangement for the latter could not be used. In that case, reflections from the hard-surface floor would have interfered with the overhead geometric farfield measurements. The microphones were consequently pole mounted, with their faces pointed at, and perpendicular to, the engine-centerline axis. The AAPL floor was covered with its usual acoustic wedges. A previous investigation of the anechoic properties of the acoustic wedges in AAPL[b] had shown that a glancing angle of less than 30° would lead to unacceptable 'ground' reflections. This constraint, in combination with a desired array aperture, implied that the sideline arrays also needed positive vertical offsets from the engine centerline in addition to their horizontal offsets. The final-design vertical offsets were chosen such that

[b]Bozak, R. F., Private Communication, 2019

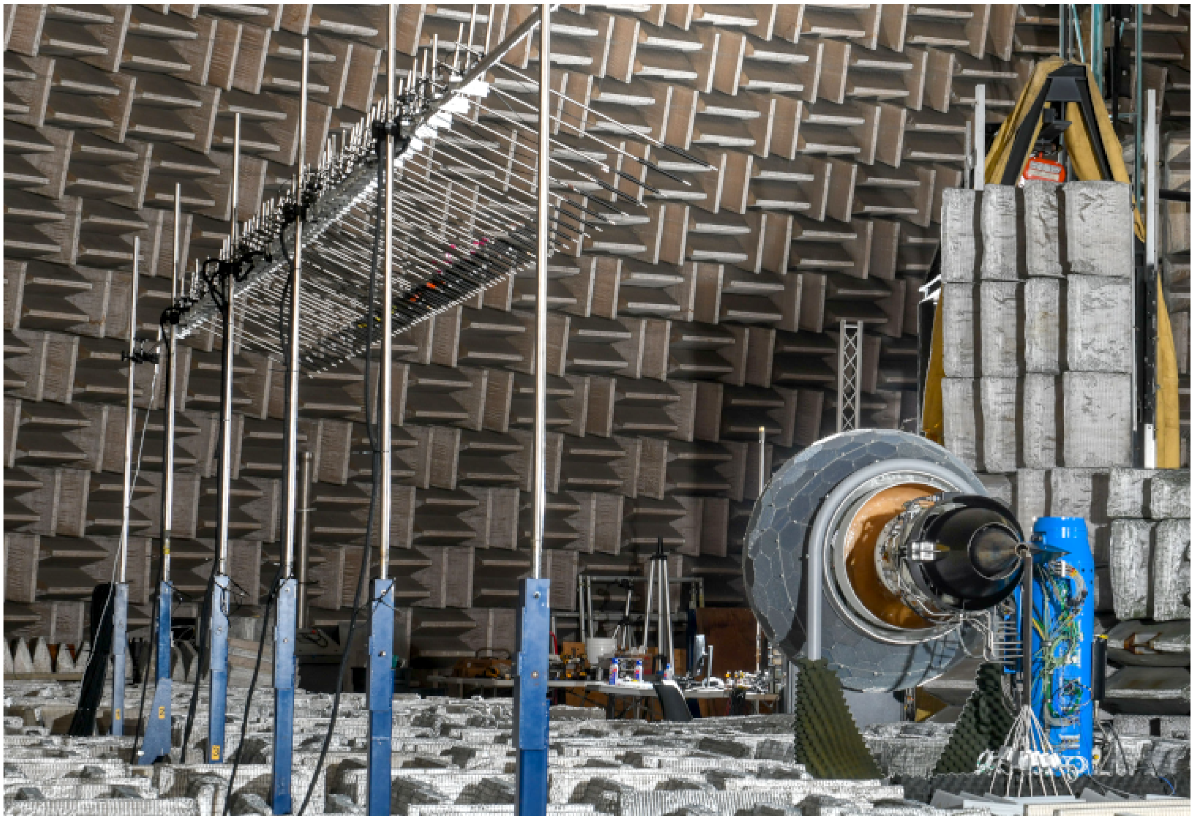

Figure 3. Aft-quadrant view of sideline-088 microphone array and DART

the microphone faces nominally would be perpendicular to the 22.25° azimuthal direction for both sideline arrays. The 61 sideline-array microphones are labeled as sensor SL101 through SL161, with the 'SL' indicating sideline and the numerical part increasing in the fore-to-aft direction. The same microphone nomenclature was used for both sideline-array configurations.

The sideline-088 array was designed to have a nominal 2.24-m (88-inch) horizontal offset from the engine-center axis and a nominal (polar) aperture of 30° to 150°, with a two-degree microphone spacing. The sideline-148 microphone array was designed to have a nominal 3.76-m (148-inch) horizontal offset from the engine-center axis and to nominally have the microphone faces perpendicular to the same 22.25° azimuthal direction as the sideline-088 array. If the sideline-148 array simply was designed as a scaled version of the sideline-088 array (i.e., same number of microphones, polar aperture, and angular microphone spacing, but at a larger horizontal offset), then the resolved frequency range of any given phased-array method applied to its data would be about 60% of the range for the corresponding sideline-088 results. This follows from the fact that the upper frequency limit of phased-array methods is essentially determined by the inverse of the largest distance between two adjacent microphones in the array. This frequency-range reduction is clearly not desirable. This problem can be remedied by adding microphones at the two extremes of the array to bring this distance below a desired maximum value. Unfortunately, no additional suitable microphones were on hand for the test campaign. Consequently, the design decision was therefore made to limit the aperture of the sideline-148 array to roughly 45° to 135° and to decrease the angular spacing at the extremes in order to roughly achieve the same upper frequency limit for phased-array methods as for the sideline-088 array. Of the 61 available microphones, 31 were used to achieve a two-degree separation in the center portion and the remaining 30 were used (in two sets of 15) to achieve a one-degree separation at the two extremes of the sideline-148 array, respectively.[c]

---

[c]In retrospect, it might have been better to allocate microphones to only decrease the angular spacing in the aft portion of the array since the DART noise field is aft-dominant, but this speculation is left for future investigation

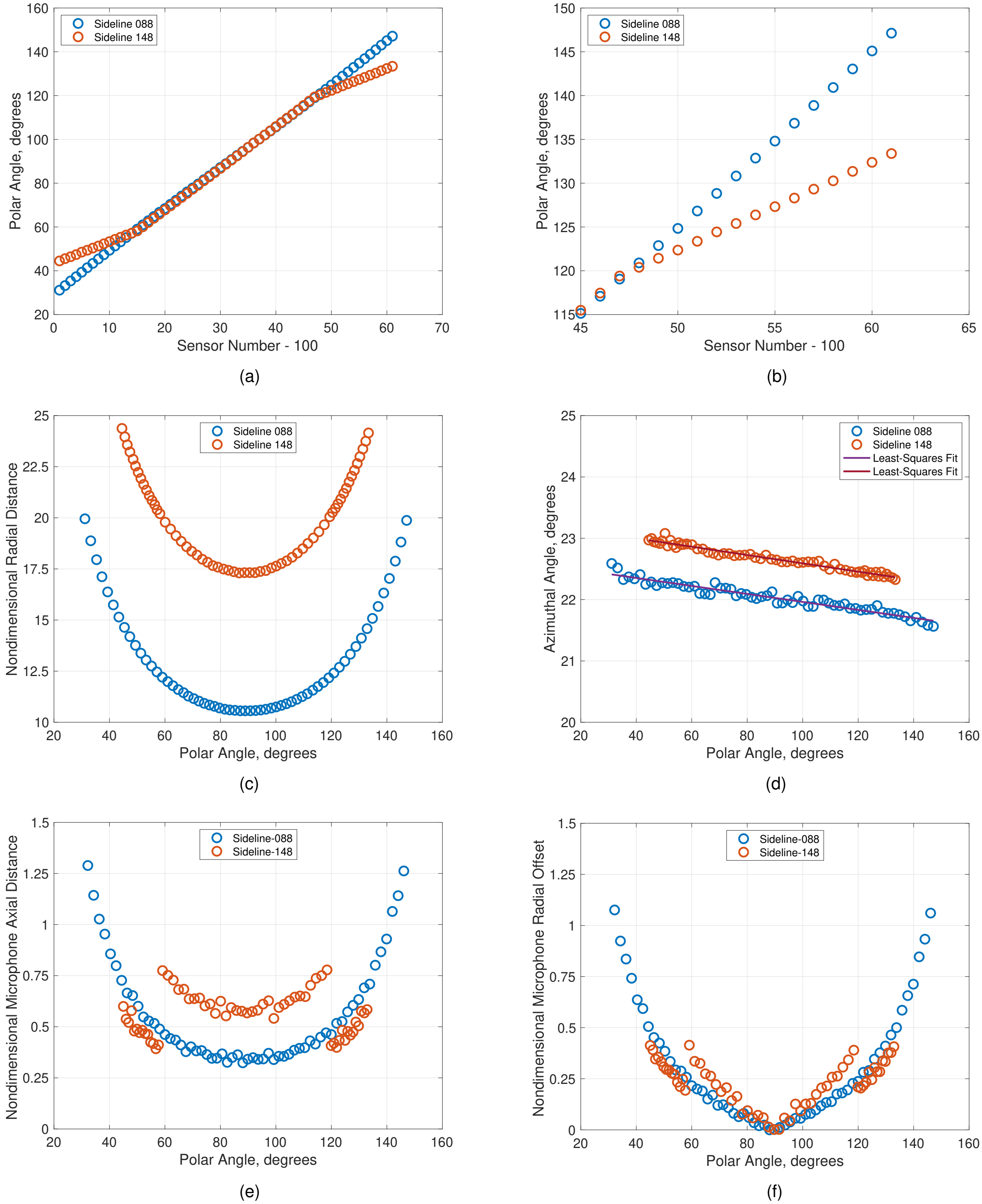

Figure 4. Sideline microphone arrays 088 (blue) and 148 (red): (a) and (b) – polar angle versus sensor index, (c) – nondimensional radial distance versus polar angle; (d) – azimuthal angle versus polar angle; (e) – nondimensional microphone-pair axial spacing versus averaged polar angle; (f) – nondimensional microphone-pair radial offset versus averaged polar angle

Figure 4(a) and (b) show the as-implemented polar angle of the two alternate sideline arrays as a function of the microphone/sensor index, with the latter panel zoomed in on the aft positions. These two subfigures indicate which polar directions are common to both builds, as well as give a visual indication of the associated level of the accuracy. The actual polar apertures of the sideline-088 and sideline-148 arrays turned out to be 31–147° and 45–133°, respectively. Figure 4(c) and (d) depict the nondimensional radial distance and azimuthal angle, respectively, as functions of the polar angle. The nondimensional radial distance fall in the ranges of about 11–20 and 17–24 for the sideline-088 and sideline-148 arrays, respectively. These radial distances are large enough to be considered as being in the acoustic farfield, i.e., a flow region where hydrodynamic fluctuations are negligible, but not large enough to be representative of a geometric-farfield location. The azimuthal angle, see panel (d), shows a slight decrease with increasing polar angle for both arrays as well as a systematic offset between the two designs. Least-square linear fits of the data are indicated by solid lines. The slopes were found to be nearly identical at -0.0065 and -0.0068 for the sideline-088 and sideline-148 arrays, respectively. The average, or essentially systematic, offset of the two fits was found to be 0.632°. The change of the azimuthal angle over the polar-angle range for each array, as well as the difference between the two arrays, are all actually quite small. Consequently, the average azimuthal angle for the 90° polar direction can be used to characterize both sideline arrays. This value is 22.34° and is remarkably close to the desired value of 22.25°.

Figure 4(e) shows the nondimensional axial offset, which is also the nondimensional distance, between adjacent microphones for each of the two arrays. The corresponding microphone-pair nondimensional radial offsets are shown in Fig. 4(f). The abscissa in these last two subfigures is the averaged polar angle of each microphone pair. These two panels contain information that could be of use in determining/estimating the valid frequency range for a phased-array method applied to the data, but this topic will not be further discussed here.

PCB Model 378C01 1/4-inch free-field prepolarized microphones were used in sideline-array positions SL101–SL130. These microphones were routed through four 8-channel PCB Model 483C50 sensor signal conditioners. Each PCB-483C50 channel is A/C coupled by design (10 s time constant, i.e., 0.1 Hz highpass-filter frequency) and was set to unity gain. GRAS type 46BE 1/4-inch prepolarized condenser-type microphones were used in the remaining sideline-array positions, SL131–SL161. These microphones were directly connected to the analog-to-digital conversion (ADC) system.

2.3 *Core-Nozzle-Exit Circumferential Array*

Eight Kulite® XCS-190-5D 5 psi (34.47 kPa) differential unsteady pressure transducers, each in the infinite-tube-probe (ITP) arrangement, were installed at the core-nozzle exit providing engine-internal measurements. Figure 5 shows the DART with the instrumented tailcone installed, with panel (c) schematically showing the location of the ITP ports in more detail. The ITP ports have uniform 45° azimuthal spacing. They are labeled NE801 through NE808, with the 'NE' indicating (core) nozzle exit. In the standard configuration, sensor port NE801 is in the twelve o'clock (90°-azimuthal) position and the numerical identifier increases in the counter-clockwise (positive-azimuthal) direction in the panel (c) view. There are two additional instrumentation ports, offset ±22.5° from the NE801 port, allowing for supplementary instrumentation. In the clocked configuration, the circumferential array is rotated -22.5°.

The ITP sense lines are all 1.22 m (48 inch) long. They are routed, see Fig. 5, through the core-nozzle center body into an simple symmetric airfoil while crossing the core and fan streams, each leading to a block where a pressure transducer is flush-mounted to the inner wall of the sense line. On the other side of each transducer tee is a 15.24 m (50 ft) long 'infinite' line with a capped termination. This line is sufficiently long to eliminate effects on the measurements by reflections from the end conditions, see [7]. The inner diameter of 4.93 mm (0.194 inch) is maintained throughout to avoid any cross-sectional area discontinuities, which would lead to pressure reflections/distortions. The transducers' 5-psi differential pressure range made it acceptable to vent each transducer's reference-pressure side to atmospheric conditions. The ideal transfer function (i.e., no reflections from the infinite-line end and no sensor-tee volume effects) for this ITP design is illustrated in Fig. 6. Based on the results in Boyle et al. [7], the use of this approximation is adequate for the present situation.

The pressure transducers were provided constant-voltage excitation by a Precision 28118-FX02-LP4FP-T 8-channel bridge-conditioner card. Six-wire cables were employed for each channel, with the three pairs providing excitation voltage, excitation monitoring, and signal transfer. The card also performed analog gain, with its built-in programmable lowpass filter bypassed, prior to the transducer output signals entering the ADC system.

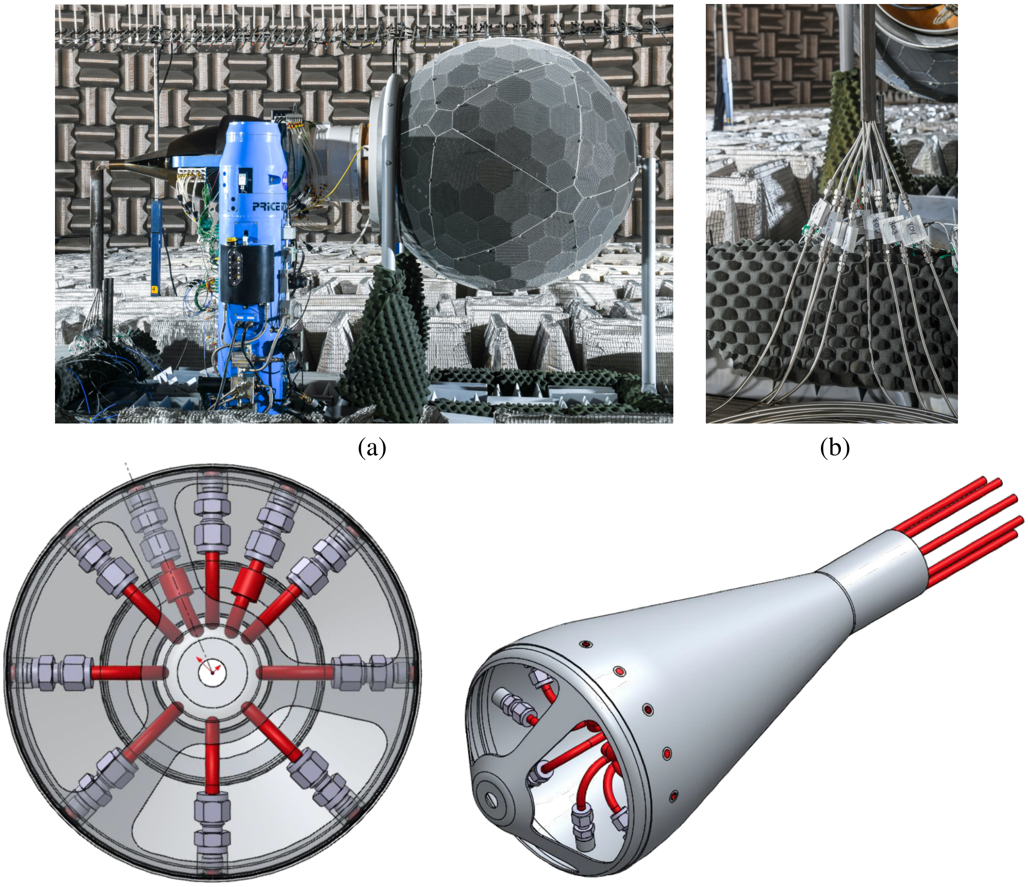

(a) (b) (c) (d)

Figure 5. (a) DART with instrumented tailcone; (b) ITP transducer tees; (c) tailcone instrumentation ports, downstream view; (d) tailcone schematic

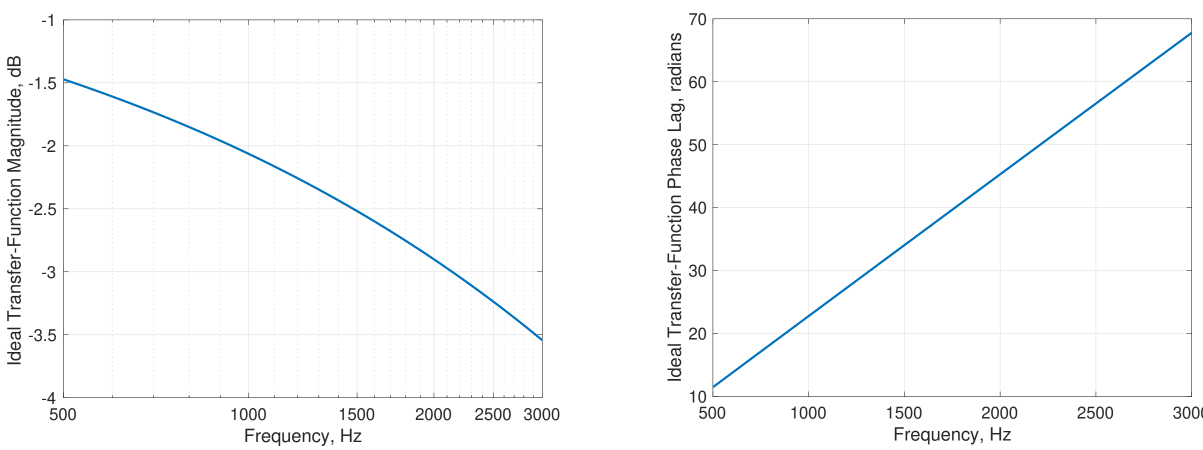

(a) (b)

Figure 6. Ideal ITP transfer function [7]: (a) – magnitude; (b) – phase lag

2.4 *Data Acquisition and General Processing*

The 85 microphone signals and the 8 ITP signals are simultaneously digitized at 100,000 samples per second utilizing a a National Instruments^{TM} (NI) PXIe-1082 chassis, populated with NI 4499 and 4498 analog-to-digital converter cards. See Appendix B for layout details. The total observation time is 60 s at each experimental test point. Each individual time series thus contains 6 million data points, i.e. 558 million data points are obtained for each test condition. In general, narrowband spectra are computed, as in [2], using an FFT length of 16,384 points (corresponding approximately to a 6.1 Hz frequency resolution or binwidth), Hamming windowing, and a 50 percent data-segment overlap. The resulting narrowband spectra are the average of a large number of realizations (over 700 instantaneous spectra). Auto-spectra are computed using both the built-in capabilities of the NI LabVIEW software that is used to control the data acquisition and post-test using MATLAB scripts and routines. Cross-spectra, presented and utilized in other reports, are computed using MATLAB with time-of-flight corrections applied to the microphone signals when appropriate.

Select engine mean-line data—such as ambient conditions, turbofan engine-station data, and engine-performance parameters—are recorded by an engine-data system at a sampling rate of 1 Hz. The engine-data system typically provided trigger events for the high-speed data-acquisition system at the beginning of each test-point sequence in order to determine the clock offset between the two systems.

2.5 *Typical Test-Point Sequence and Test Matrix*

For each experimental configuration, the full authority digital engine control (FADEC) unit of the DART executed a program that runs through a sequence of predefined, monotonically increasing, engine-power settings, with each setting set to be held for 120 seconds. The control program starts at idle (33%) and dwells at each of the power settings shown in Table 1. After having reached the maximum allowable power setting (limited by the ambient temperature), it then returns to idle, and the sequence is then repeated once. The sequence also contains two test points with the engine off, but with support systems (such as the oil pump, etc.) running, for background-noise assessment. The power setting represents the ratio of the corrected fan speed on condition to that at a particular design point. Equivalently, it can be expressed in terms of low-pressure-spool shaft speeds as

Table 1. Typical DART test-point/engine-power sequence

Test Point	1	2	3	4	5	6	7	8	9	10	11	12	13	14	15	16
Power, %	33	50	60	70	80	90	Max	33	50	60	70	80	90	Max	0	0

$$\text{power} = N_{\text{Lc}}/N_{\text{Ld}}\,, \tag{1}$$

where $N_{\text{Lc}} = N_{\text{L}}\sqrt{T_{\text{SLS}}/T_{\text{amb}}}$ is the temperature-corrected low-pressure-shaft speed and N_{Ld} is the design-point (corrected) shaft speed; N_{L} is the actual shaft speed, $T_{\text{SLS}} = 288.15$ K is the sea-level standard temperature, and T_{amb} is the ambient temperature (also in K) during a test point. The allowable maximum power in Table 1 is given by

$$\text{Max} = \min(92.5, N_{\text{La}}\sqrt{T_{\text{SLS}}/T_{\text{amb}}}/N_{\text{Ld}})\,, \tag{2}$$

where N_{La} is a facility determined maximum allowable actual low-pressure-spool shaft speed. Consequently, the maximum-power set point is reduced for sufficiently high ambient temperatures. The FADEC program automatically enforces the limitation defined in Eq. (2).

Figure 7 shows a typical low-pressure-spool shaft-RPM profile corresponding to Table 1. The blue curve shows the actual shaft speed, N_{L}, as reported by the engine-data system/FADEC, versus time expressed as a fraction of 24-hour day (a common timestamp used by data-acquisition systems operating under Microsoft Windows). The red lines show the average shaft speed during each data-acquisition event. The two brief excursions away from idle at the beginning of the profile were executed to allow for time synchronization between the high-rate and slow-rate acoustic-data and mean-line-data acquisition systems, respectively.

Boyle et al. [2] found that the engine under FADEC control performed quite repeatably in maintaining shaft speed for a given set point. The actual low-speed-shaft rotation rate, N_{L}, had an RPM deviation of less than 0.04% and

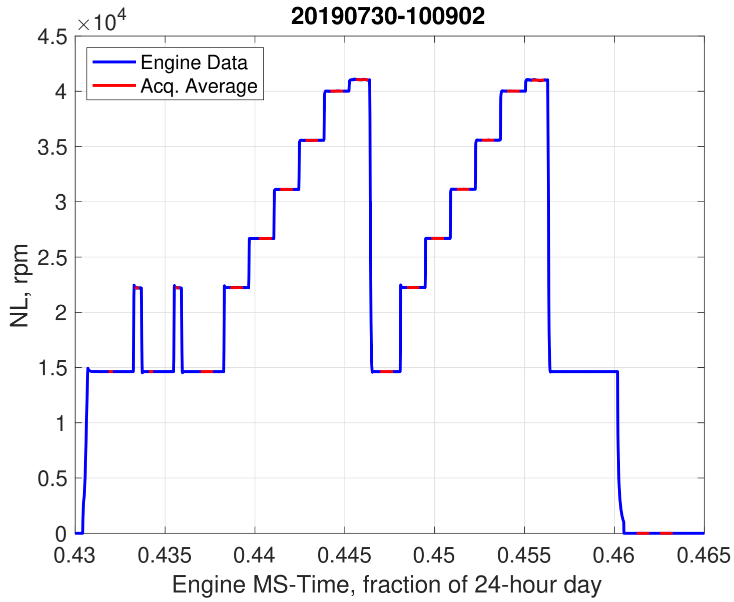

Figure 7. Typical DART low-pressure-spool RPM profile

its maximum observed deviation was less than 0.1%. Typical shaft-passing frequencies for the high-pressure spool, SPF_{H}, low-pressure spool, SPF_{L}, and the fan shaft, SPF_{F}, as well as blade-passing frequencies for the fan, BP_{F}, and low-pressure turbine, BP_{L}, can be seen in Boyle et al. [2, Table 3]. Note that the BP_{L} tone typically only falls within the 10 kHz frequency range for the idle power settings.

The test matrix using the automated engine-control sequence is illustrated in Table 2. The 'baseline' notation implies that the original non-instrumented tailcone was used for those test points. Further test-matrix details are given in Appendix C

Table 2. Automatic-Sequence Test Matrix

Date	Type	Test Points	Power Levels, %	Tailcone	Sideline Array
2019-07-30	Repeated Automatic	1–7; 8–14	33, 50, 60, ..., 90, 92.3; 33, 50, 60, ..., 90, 92.3	Baseline	LA088
2019-07-30	Background	15; 16	0; 0	Baseline	LA088
2019-08-01	Repeated Automatic	1–7; 8–14	33, 50, 60, ..., 90, 92.5; 33, 50, 60, ..., 90, 92.5	Standard	LA088
2019-08-01	Background	15; 16	0; 0	Standard	LA088
2019-08-01	Repeated Automatic	17–23; 24–30	33, 50, 60, ..., 90, 92.3; 33, 50, 60, ..., 90, 92.1	Clocked	LA088
2019-08-01	Background	31; 32	0; 0	Clocked	LA088
2019-08-07	Repeated Automatic	1–7; 8–14	33, 50, 60, ..., 90, 92.5; 33, 50, 60, ..., 90, 92.5	Clocked	LA148
2019-08-07	Background	15; 16	0; 0	Clocked	LA148
2019-08-07	Repeated Automatic	17–23; 24–30	33, 50, 60, ..., 90, 92.3; 33, 50, 60, ..., 90, 92.0	Standard	LA148
2019-08-07	Background	31; 32	0; 0	Standard	LA148
2019-08-07	Background, no aux	35; 36	0; 0	Standard	LA148
2019-08-08	Repeated Automatic	1–7; 8–14	33, 50, 60, ..., 90, 92.5; 33, 50, 60, ..., 90, 92.5	Baseline	LA148
2019-08-08	Background	15; 16	0; 0	Baseline	LA148
2019-08-08	Background, door closed	35; 36	0; 0	Baseline	LA148

3 Acoustic Data

For each test point, the NI system is programmed to produce a text (ASCII) 'header' file for each chassis slot in use, and two binary files for each slot channel. One of the binary files contains the slot-channel time history in physical units (Pa). The other contains the corresponding narrowband sound-pressure-level (*SPL*) spectrum (dB) as computed during the acquisition. The header file contains various information such as time and date, sampling rate, nominal acquisition time, signal-processing parameters for the concurrent *SPL* computation, and sensor information for active channels.

For convenience, this information and data are, for each test point, combined with test-matrix, instrumentation-layout, and sensor-location information, and then repackaged into self-contained files corresponding to each array in use. The resulting files are MATLAB files version 7.3—Hierarchical Data Format version 5 (HDF5)[d]—using the naming convention 'DART*YYYYMMDD_XXXX*-tp*NNN*.mat,' where YYYYMMDD is the test-point date, XXXX can have the values FFOVH, LA088, LA148, or NEITP indicating the array (farfield, sideline, and core-nozzle-exit), and NNN is simply the test-point number. For example, 'DART20190730_LA088_tp001.mat' contains the test-point-1 data for the sideline-088 array from August 30, 2020, see Appendix D for details. Note that the nomenclature 'LA' is used in this context to avoid conflict/confusion with the sideline-array microphone-labeling scheme used here.

4 Summary

This document describes the experimental setup, test matrix, and the data structure of the acquired acoustic data for the DGEN Aeropropulsion Research Turbofan (DART) source-diagnostic test (SDT) in the NASA Glenn Research Center Aero-Acoustic Propulsion Laboratory (AAPL) carried out during July–August of 2019. The DART-SDT campaign continued the exploration and documentation of the DART core/combustor noise begun in an earlier baseline test [2], but now with more extensive instrumentation, in order to answer questions raised by the previous investigation, as well as to further enhance the understanding of propulsion-noise sources and their impact on airport community noise resulting from the operation of civilian transport aircraft. The extensive instrumentation used during this test campaign yielded a large of amount of simultaneously-acquired acoustic data.

Boyle et. al [8] demonstrated that the acoustic data is of high-quality and also performed a modal decomposition of the unsteady pressure field at the core-nozzle exit. The latter confirmed observations and conclusions based on their previous work [2]. Further detailed analysis of the data is in progress, which includes the application of advanced source-separation and modal decomposition techniques in order to illuminate the core/combustor-noise source structure and propagation to the farfield, and will be reported in the near future.

APPENDICIES

A Acoustic-Sensor Coordinates

The microphone locations are described using a spherical coordinate system, with the origin located on the engine centerline at the core-nozzle-exit plane. As usual, the radial coordinate is simply the distance from a location to the origin. Here, the fixed zenith axis is the engine centerline, with the positive direction taken to be towards (and beyond) the engine inlet. The so-called reference plane contains the origin and its normal vector points in the positive zenith direction. The polar angle is measured relative to the positive zenith axis and, consequently, is zero in the inlet direction. The azimuthal coordinate is the angle of the orthonormal projection of a point onto the reference plane measured relative to the positive (here) horizontal axis of that plane. It follows that the azimuthal angle is zero in the engine port-side (left-hand side facing forward) horizontal plane. The 90° azimuthal direction, consequently, corresponds to the positive vertical direction. The relationship between the corresponding local cartesian coordinate system and the spherical one is hence

$$x = r\cos\phi\,, \quad y = r\sin\phi\cos\theta\,, \quad z = r\sin\phi\sin\theta\,,$$

where (x, y, z) are the engine axis, horizontal and vertical coordinates, and (r, ϕ, θ) are the radial, polar and azimuthal coordinates. This local cartesian system is related to the facility-based coordinate system used in AAPL simply by an origin shift.

[d] https://en.wikipedia.org/wiki/Hierarchical_Data_Format, Retrieved 2020-09-17.

The coordinates of the acoustic-sensor layout are documented in the file ‘DART2019-SensorLayout.mat.’ The nested structure of this MATLAB file (version 5) is illustrated in Figs. A 1– A 3. The top-level structure, see Fig. A 1, contains members (all but one are themselves structures) that describe the source file for the raw AAPL-based coordinates, these raw coordinates, the sensor configuration, and the corresponding engine-centric spherical coordinates for each sensor. For example, see Fig. A 2, the substructure ‘sensor_loc.raw_geometry’ contains the cartesian AAPL coordinates of all the overhead microphone locations in the structure ‘overhead’, with units as indicated in ‘units’ (unit_system = ‘eu’ means that U.S. customary engineerng units are used), etc.; the substructure ‘sensor_loc.config’ provides the numerical index associated with a particular sensor (‘sensid’) and the corresponding name (‘sensname’), say 101 and SL101; and the substructure ‘sensor_loc.spherical’ contains structures that provide the core-exit-plane-based spherical coordinates of the sensors, see Fig. A 3. The engine-local cartesian coordinates are also provided for the two alternate sideline arrays. Radial and cartesian sideline-array coordinates are provided in both nondimensional and dimensional forms, eg. the variables r, r_ft, and r_m hold the radial coordinate in nondimensional form, in feet, and in meters, respectively. Polar and azimuthal angles are in degrees.

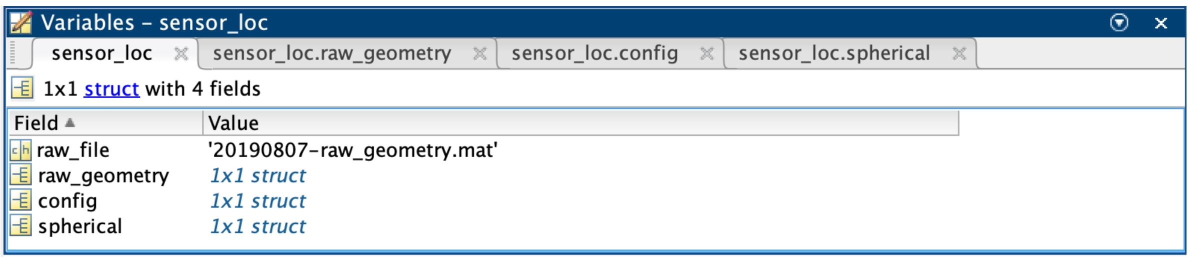

Figure A 1. The top level of the nested structure 'sensor_loc' stored in the file DART2019-SensorLocations.mat

B High-Speed Instrumentation Layout

The NI PXI chassis, used for the high-data-rate acoustic acquisition, is populated with 16-channel, 24-bit ADC cards in slots 2–7 (the chassis controller occupies slot 1). The information needed to associate a particular sensor with a specific ADC card (‘ADCSlot’) and corresponding card channel (‘AIChannel’), as well other information, is stored in the MATLAB file (version 5) ‘DART2019-InstrumentationLayout.mat,’ see Fig. B 1.

C Test Matrix

Further details of the automated-sequence test matrix (see Table 2 in Section 2.5) are stored in the file ‘DART2019-AutomatedSequenceTestMartix.mat.’ Figure C 1 illustrates the contents of this MATLAB file. It contains top structures associated with particular testing days (four). Each such structure contains test date, identifiers for acoustic and mean-line data, and substructures for each test point. Figure C 2 shows the details of one such substructure. It indicates tailcone and sideline-array configurations, test-point number and type, requested power setting in terms of percent corrected fan speed, and acoustic-data-acquisition start time, duration in seconds, and sample rate in Hertz. The environmental and (a very restricted number of) engine parameters shown are obtained by averaging output from the slow (1 Hz) engine-data system over the duration of the high-speed acquisition. The environmental variables are: P_{amb}—the ambient pressure (kPa) measured by a ‘floor-level’ sensor located near the base of the engine pylon; T_{amb}, T_{C15}, and T_{ext}—three measures of the ambient temperature (K) using sensors located behind the engine inlet lip, on the pylon, and on the sideline array; and $rHum$—relative humidity in percent measured at the sideline array. The engine parameters shown are the actual low- and high-pressure-spool shaft speeds N_{L} and N_{H}, the actual corrected fan speed N_{FANc} (all in rpm), and the actual engine power (see Eq. 1). Except for the shaft speeds and power, no (other available) engine internal mean-line or performance parameters are reported here.

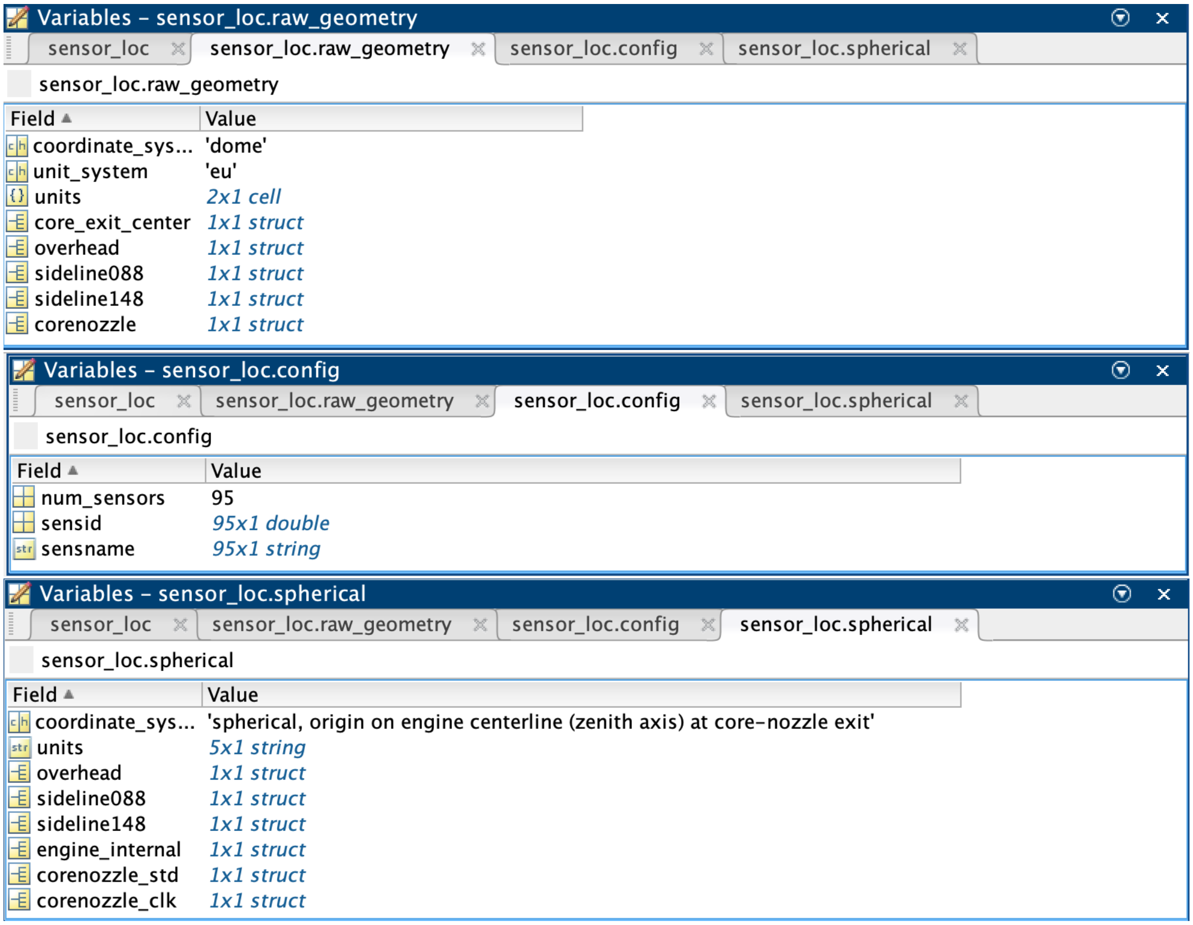

Figure A 2. The second levels of the nested structure 'sensor_loc' stored in the file DART2019-SensorLocations.mat

D Acoustic-Data-File Structure

Using the file DART20190730_LA088_tp001.mat as an illustrative example, the general nested structure of the acoustic-data files is shown in Figs. D 1– D 5. The top-level structure 'AcousticData', see Fig. D 1, has substructures containing test and configuration information, as well as substructures for each sensor holding information and data. As can be seen in Fig. D 2, the substructure 'header' contains overall test information and the substructure 'configuration' holds information for the specific test point. In this particular file, there are 61 substructures corresponding to the sensors SL101–SL161. Figure D 3 shows the contents of the substructure 'SL101'. It contains two third-level structures (of the AcousticData structure), namely 'header' with sensor information and 'coordinates' holding the sensor location. It also contains the physical time history (Pa), the narrowband frequencies (Hz), and narrowband *SPL* spectrum (dB) in the variables 'this', 'freq', and 'spec', respectively. The third-level substructures are illustrated in Fig. D 4. The fourth-level substructure 'slot_header', see Fig. D 5, contains mostly redundant data and is included only for completeness. The third-level substructure 'header' provides, among other information, slot, card-type, analog-input channel (0–15) and sensor name, brand, model, sensor type ('Voltage' or 'TEDS') serial number, sensitivity (Pa/V) and AC/DC (1/0) input coupling. Names of relevant (originally) NI-system produced files (see Section 3) are given by the variables 'hisfile', 'splfile', and 'hdrfile' (in the substructure 'slot_header') for information only—all data and information from these files are incorporated in the 'AcousticData' structure. The third-level substructure 'coordinates' holds the radial coordinate, nondimensionalized using the core-nozzle exit outer diameter, and the polar and azimuthal angles in degrees.

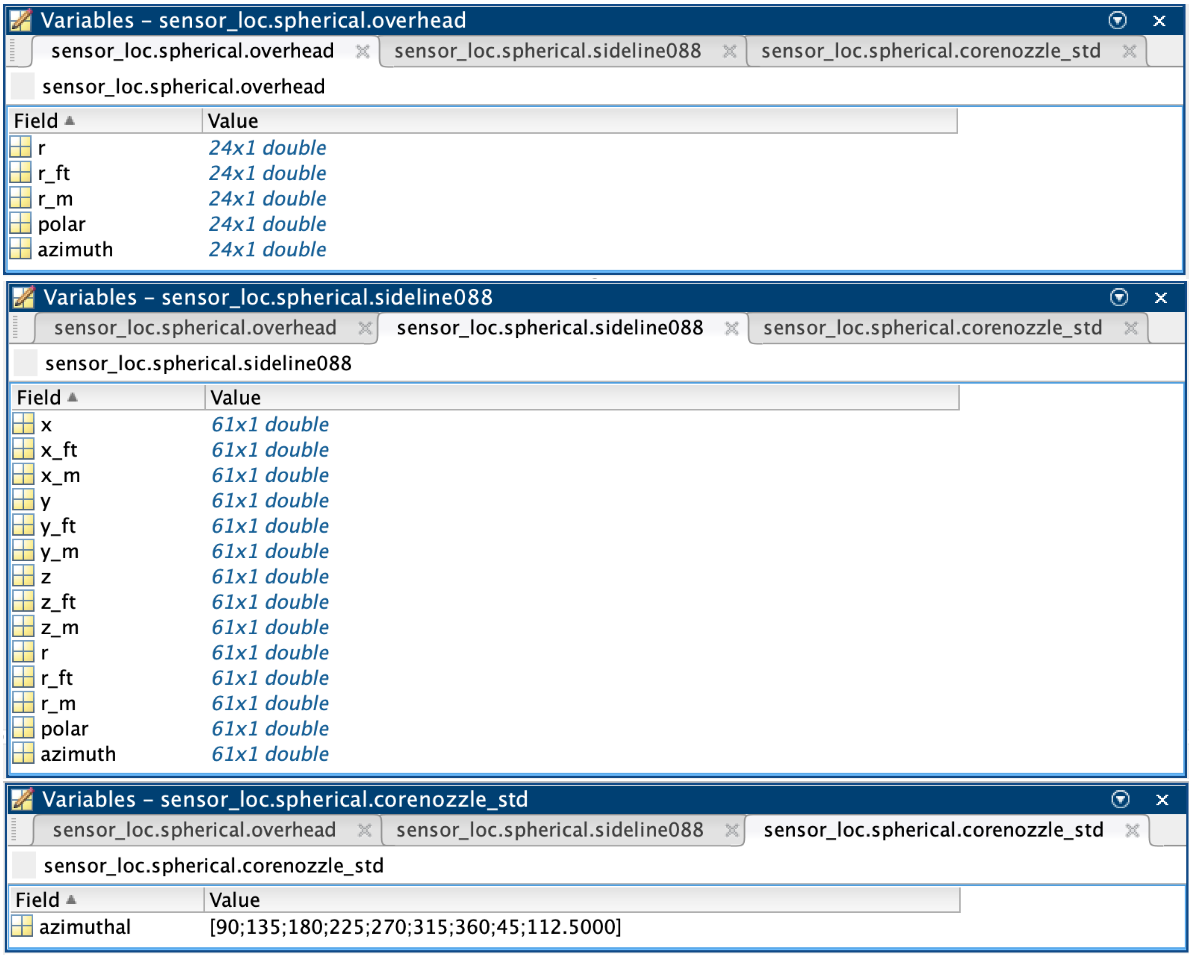

Figure A 3. Details of the nested substructure 'sensor_loc.spherical' stored in the file DART2019-SensorLocations.mat

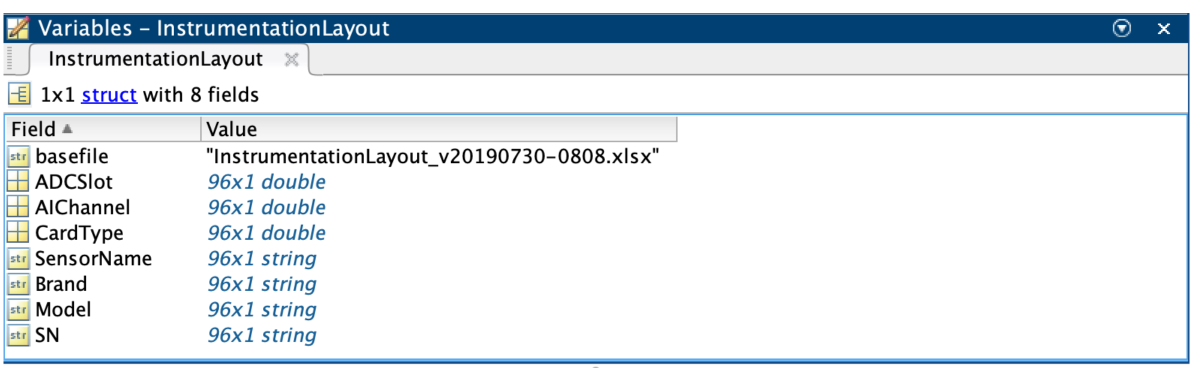

Figure B 1. The instrumentation layout is stored in the file DART2019-InstrumentationLayout.mat

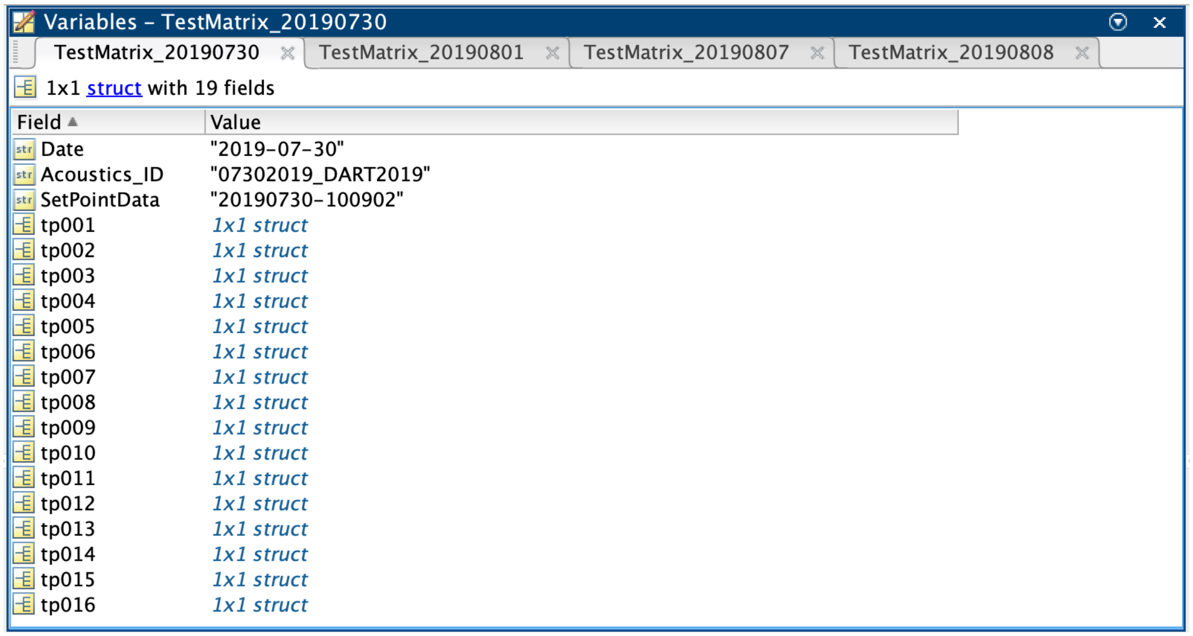

Variables – TestMatrix_20190730

TestMatrix_20190730 | TestMatrix_20190801 | TestMatrix_20190807 | TestMatrix_20190808

1x1 struct with 19 fields

Field	Value
Date	"2019-07-30"
Acoustics_ID	"07302019_DART2019"
SetPointData	"20190730-100902"
tp001	1x1 struct
tp002	1x1 struct
tp003	1x1 struct
tp004	1x1 struct
tp005	1x1 struct
tp006	1x1 struct
tp007	1x1 struct
tp008	1x1 struct
tp009	1x1 struct
tp010	1x1 struct
tp011	1x1 struct
tp012	1x1 struct
tp013	1x1 struct
tp014	1x1 struct
tp015	1x1 struct
tp016	1x1 struct

Figure C 1. Details of information stored in the file DART2019-AutomaticSequenceTestMatrix.mat

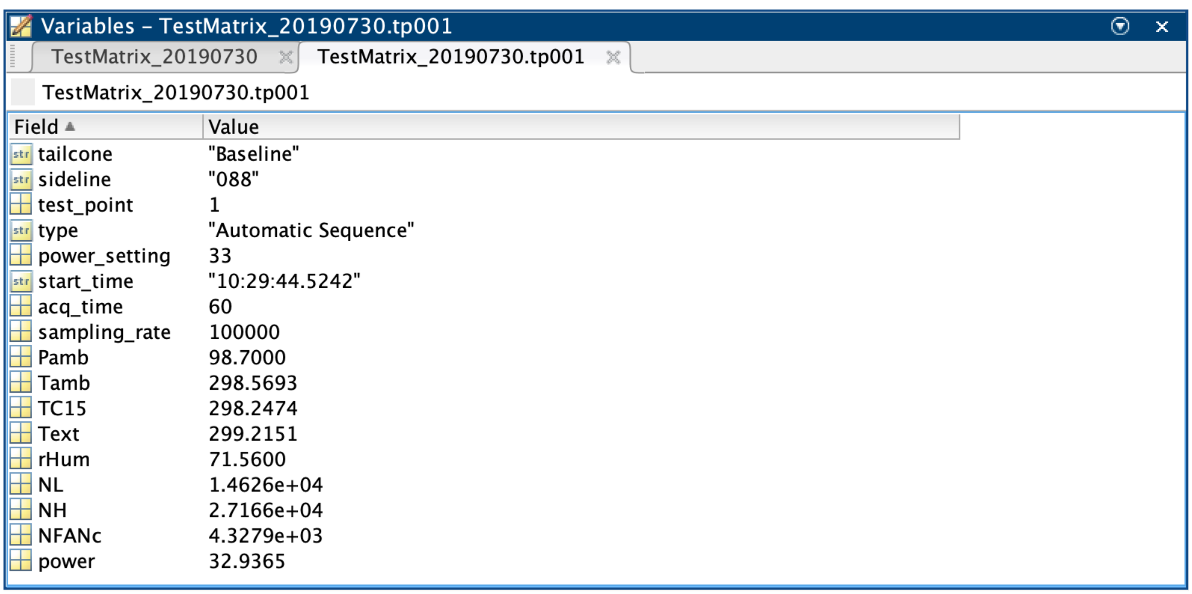

Variables – TestMatrix_20190730.tp001

TestMatrix_20190730 | TestMatrix_20190730.tp001

TestMatrix_20190730.tp001

Field	Value
tailcone	"Baseline"
sideline	"088"
test_point	1
type	"Automatic Sequence"
power_setting	33
start_time	"10:29:44.5242"
acq_time	60
sampling_rate	100000
Pamb	98.7000
Tamb	298.5693
TC15	298.2474
Text	299.2151
rHum	71.5600
NL	1.4626e+04
NH	2.7166e+04
NFANc	4.3279e+03
power	32.9365

Figure C 2. Example substructure in DART2019-AutomaticSequenceTestMatrix.mat

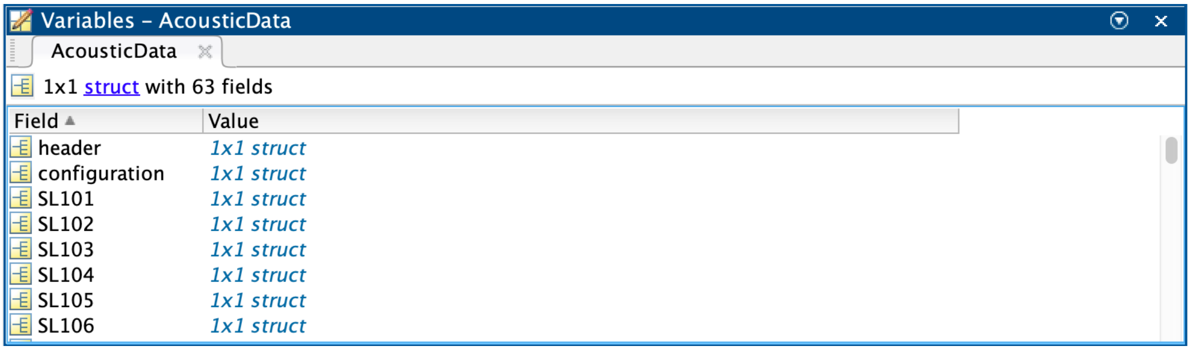

Variables – AcousticData

AcousticData

1x1 struct with 63 fields

Field	Value
header	1x1 struct
configuration	1x1 struct
SL101	1x1 struct
SL102	1x1 struct
SL103	1x1 struct
SL104	1x1 struct
SL105	1x1 struct
SL106	1x1 struct

Figure D 1. The top level of the nested structure ’AcousticData’ stored in the HDF5 file DART20190730_LA088_tp001.mat

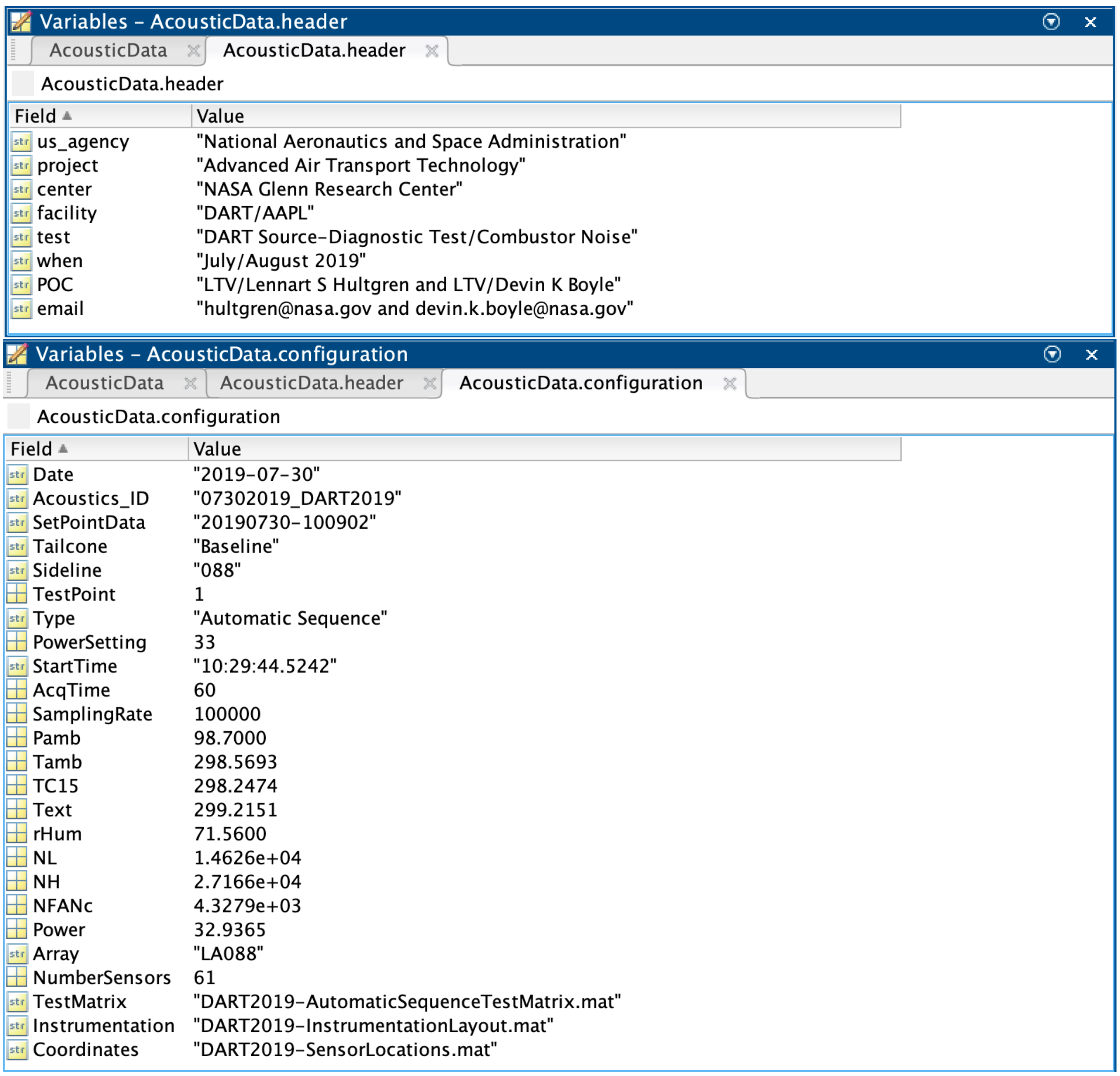

Variables – AcousticData.header

AcousticData | AcousticData.header

AcousticData.header

Field	Value
us_agency	"National Aeronautics and Space Administration"
project	"Advanced Air Transport Technology"
center	"NASA Glenn Research Center"
facility	"DART/AAPL"
test	"DART Source–Diagnostic Test/Combustor Noise"
when	"July/August 2019"
POC	"LTV/Lennart S Hultgren and LTV/Devin K Boyle"
email	"hultgren@nasa.gov and devin.k.boyle@nasa.gov"

Variables – AcousticData.configuration

AcousticData | AcousticData.header | AcousticData.configuration

AcousticData.configuration

Field	Value
Date	"2019–07–30"
Acoustics_ID	"07302019_DART2019"
SetPointData	"20190730–100902"
Tailcone	"Baseline"
Sideline	"088"
TestPoint	1
Type	"Automatic Sequence"
PowerSetting	33
StartTime	"10:29:44.5242"
AcqTime	60
SamplingRate	100000
Pamb	98.7000
Tamb	298.5693
TC15	298.2474
Text	299.2151
rHum	71.5600
NL	1.4626e+04
NH	2.7166e+04
NFANc	4.3279e+03
Power	32.9365
Array	"LA088"
NumberSensors	61
TestMatrix	"DART2019–AutomaticSequenceTestMatrix.mat"
Instrumentation	"DART2019–InstrumentationLayout.mat"
Coordinates	"DART2019–SensorLocations.mat"

Figure D 2. Second-level substructures ’header’ and ’configuration’ stored in the HDF5 file DART20190730_LA088_tp001.mat

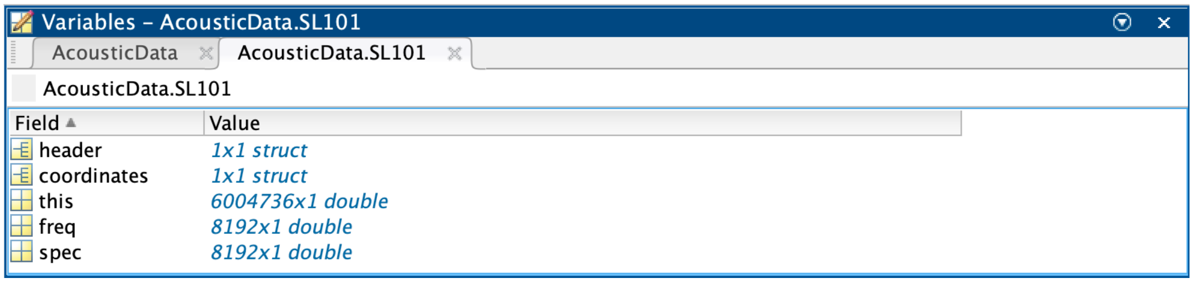

Figure D 3. Details of the second-level substructure 'SL101' stored in the HDF5 file DART20190730_LA088_tp001.mat

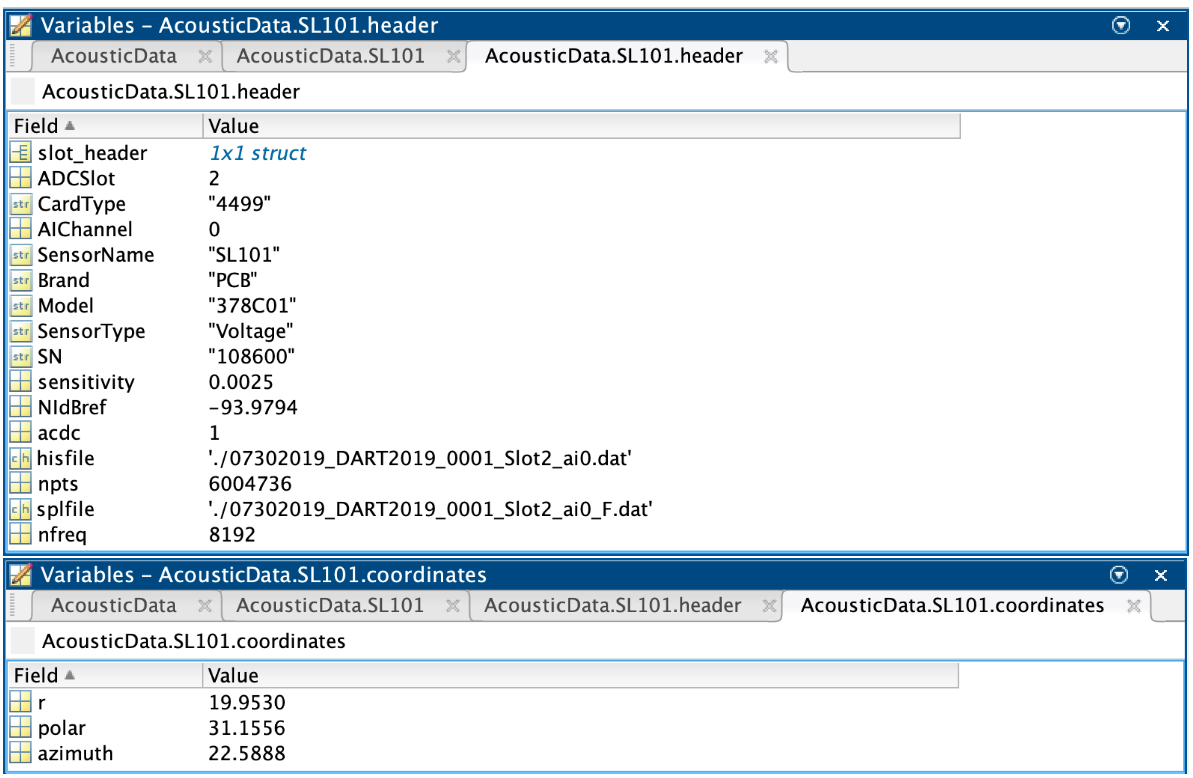

Figure D 4. Third-level substructures 'header' and 'coordinates' stored in the HDF5 file DART20190730_LA088_tp001.mat

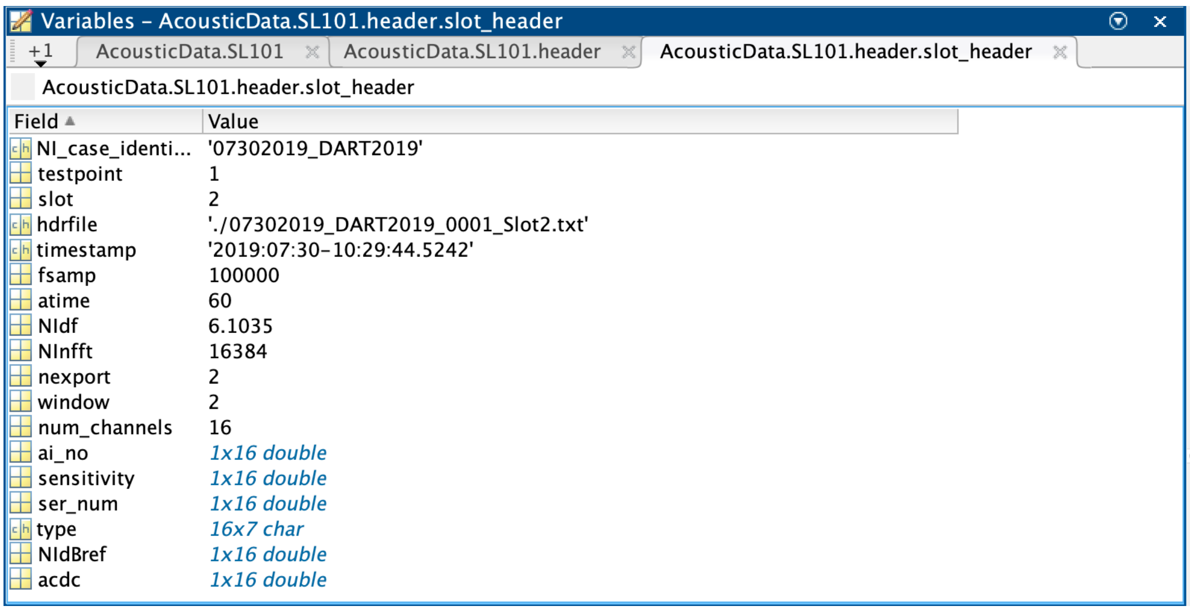

Figure D 5. Details of the fourth-level substructure 'slot_header' stored in the HDF5 file DART20190730_LA088_tp001.mat

REFERENCES

[1] Mongeau, L., Huff, D. and Tester, B. J. "Aircraft Noise Technology Review and Medium and Long Term Noise Reduction Goals." *ICA 2013 Montreal*. Proc. Mtgs. Acoust. 19, 040041. 2013. DOI 10.1121/1.4800944.

[2] Boyle, D. K., Henderson, B. S. and Hultgren, L. S. "Core/Combustor-Noise Baseline Measurements for the DGEN Aeropropulsion Research Turbofan." AIAA Paper 2018-3281, 24th AIAA/CEAS Aeroacoustics Conference, Atlanta, Georgia. 2018. DOI 10.2514/6.2018-3281.

[3] Hultgren, L. S. "A First Look at the DGEN380 Engine Acoustic Data From a Core-Noise Perspective." Technical Report No. NASA/TM–2015-218924, NASA. 2015.

[4] Sutliff, D. L., Brown, C. A., Bayon, B. and Sree, D. "Farfield Acoustic Characteristics of the DGEN380 Turbofan Engine as Measured in the NASA Glenn Aero-Acoustic Propulsion Laboratory." AIAA Paper 2016-3006, 22nd AIAA/CEAS Aeroacoustic Conference, Lyon, France. 2016. DOI 10.2514/6.2016-3006.

[5] Soeder, R. H., Wnuk, S. P. and Loew, R. A. "Aero-Acoustic Propulsion Laboratory Nozzle Acoustic Test Rig User Manual." Technical Report No. NASA/TM–2006-212939, NASA. 2006. Restricted: Do not release on a public Web site, see NPR 2810.1A.

[6] Ahuja, K. K. "Designing Clean Jet-Noise Facilities and Making Accurate Jet-Noise Measurements." *International J. Aeroacoustics* Vol. 2, No. 3&4 (2003): pp. 371–412. DOI 10.1260/147547203322986188.

[7] Boyle, D. K., Henderson, B. S. and Hultgren, L. S. "Transfer-Function Determination for Infinite-Tube-Probe Pressure Transducers with Application to Turbofan Core/Combustor Noise." AIAA Paper 2019-2588 (NASA/TM–2019-220045), 25th AIAA/CEAS Aeroacoustics Conference, Delft, The Netherlands. 2019. DOI 10.2514/6.2019-2588.

[8] Boyle, D. K., Henderson, B. S. and Hultgren, L. S. "DGEN Aeropropulsion Research Turbofan Core/Combustor-Noise Measurements — Experiment and Modal Structure at Core-Nozzle Exit." Paper GT2020-14194, ASME Turbo Expo 2020, London, England. 2020.